4DVarNet, an end-to-end learning of variational interpolation schemes: current applications on stellite-derived data and on-going developments

Hugo Georgenthum[1]
Maxime Beauchamp[1], Ronan Fablet[1], Quentin Febvre[1], Mohamed Mahmoud Amar[1], Benjamin Carpentier[2]

[1]IMT Atlantique, France - [2]CLS, France

November 2022

Table of contents

1. Introduction
2. Method: 4DVarNet
3. Observation System Simulation Experiment
   - Experiments
   - New applications
4. Observation System Experiment
   - Experiments
5. Conclusion

Problem statement

- $\mathbf{y}(\Omega) = \{\mathbf{y}_k(\Omega_k)\}$: the partial and potentially noisy observational dataset
- $\Omega = \{\Omega_k\} \subset \mathcal{D}$, $\overline{\Omega}$ denotes the gappy part of the field and index k refers to time t_k.

Problem

Using a data assimilation (DA) state space formulation, we aim at estimating the hidden space

$$\mathbf{x} = \{\mathbf{x}_k(\mathcal{D})\}$$

based on the available observations $\mathbf{y}$

Current solutions

- Covariance-based **Kriging** (Chilès and Delfiner, 2012), **BLUE**, **OI** (Traon et al., 1998) and **SPDE**-based version (Lindgren et al., 2011)

- Model-based DA:
  Sequential assimilation, (En)KF, see e.g. (Evensen, 2009)
  Variational assimilation, (3DVar, 4DVar) (Asch et al., 2016)
  Hybrid methods

- Data-driven DA:
  Analog forecasting operator embedded in EnKF (AnDA) (Tandeo et al., 2015)
  Hybrid DA and machine/deep learning synergy: inference of unresolved scale parametrizations (Brajard et al., 2021; Bocquet et al., 2019), use of DA-based parameterizations inference in numerical models involving machine learning (O'Gorman and Dwyer, 2018; Rasp et al., 2018)

Table of contents

1. Introduction
2. Method: 4DVarNet
3. Observation System Simulation Experiment
   - Experiments
   - New applications
4. Observation System Experiment
   - Experiments
5. Conclusion

Variational model

Considering a variational data assimilation scheme Asch et al. (2016), the state analysis $\mathbf{x}^\star$ is obtained by solving the minimization problem:

$$\mathbf{x}^\star = \arg\min_{\mathbf{x}} \mathcal{J}(\mathbf{x})$$

where the variational cost function $\mathcal{J}(\mathbf{x}) = \mathcal{J}_\Phi(\mathbf{x}, \mathbf{y}, \Omega)$ is generally the sum of an observation term and a regularization term involving an operator Φ which is typically a dynamical prior:

$$\begin{aligned}\mathcal{J}_\Phi(\mathbf{x}, \mathbf{y}, \Omega) &= \mathcal{J}^o(\mathbf{x}, \mathbf{y}, \Omega) + \mathcal{J}^b_\Phi(\mathbf{x}) \\ &= \lambda_1 ||\mathbf{y} - \mathcal{H}(\mathbf{x})||^2_\Omega + \lambda_2 ||\mathbf{x} - \Phi(\mathbf{x})||^2\end{aligned}$$

with $\mathcal{H}$ the observation operator and $\lambda_{1,2}$ are predefined or learnable scalar weights. This formulation of functional $\mathcal{J}_\Phi(\mathbf{x}, \mathbf{y}, \Omega)$ directly relates to strong constraint 4D-Var Carrassi et al. (2018).

End-to-end joint learning scheme

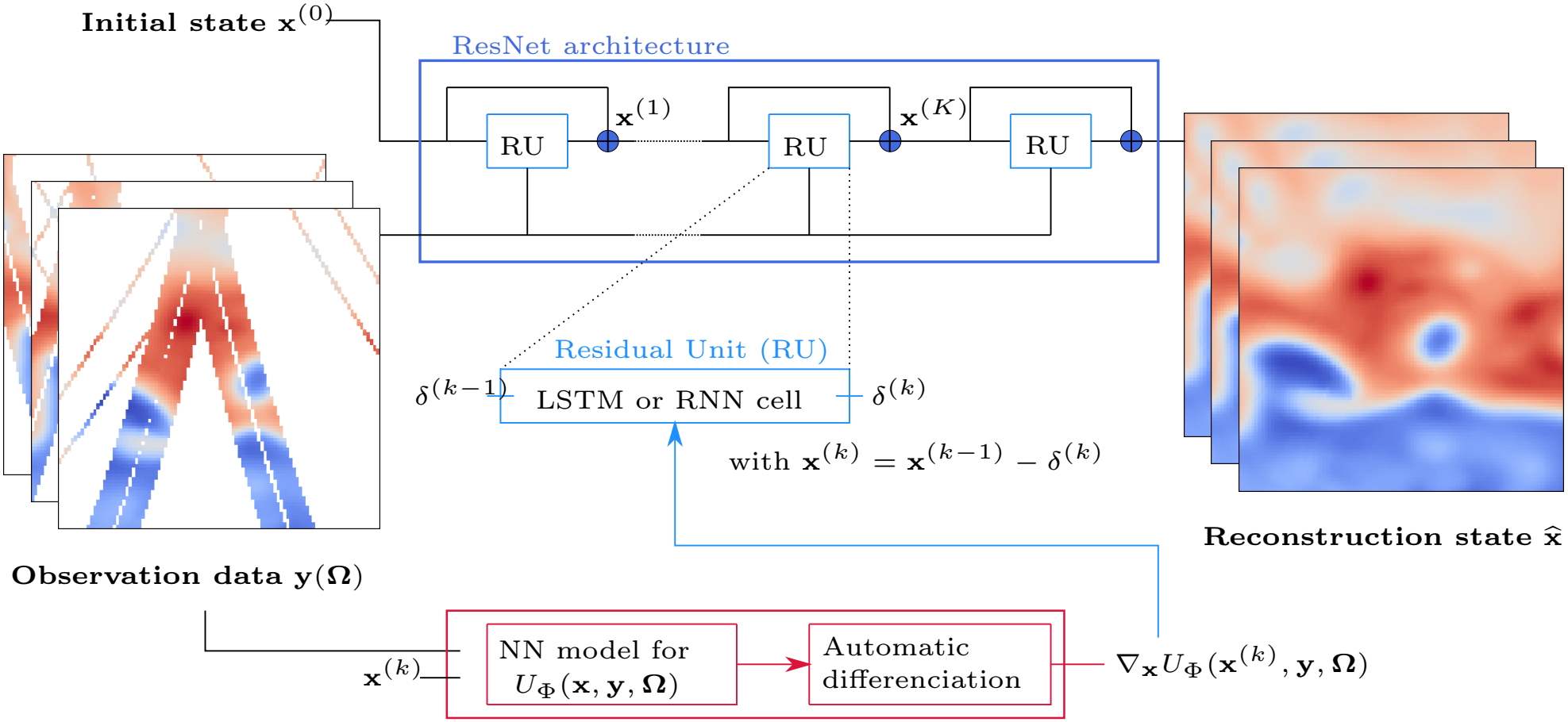

Figure: 4DVarNet

Table of contents

1 Introduction

2 Method: 4DVarNet

3 Observation System Simulation Experiment
- Experiments
- New applications

4 Observation System Experiment
- Experiments

5 Conclusion

Domain

- Ground truth dataset $\mathbf{x}$: high-resolution 1/60° NATL60 configuration of the NEMO (Nucleus for European Modeling of the Ocean) model
- A 10° × 10° GULFSTREAM region is used with downgraded resolution to 1/20°, principally led by mesoscale processes
- A 10° × 8° "open-ocean" OSMOSIS region is used with downgraded resolution to 1/20°

Figure: GULFSTREAM domain

- OSSE : pseudo-altimetric nadir and SWOT observational datasets are generated by a realistic sub-sampling satellite constellations.

Data

(a) Ground Truth (SSH)

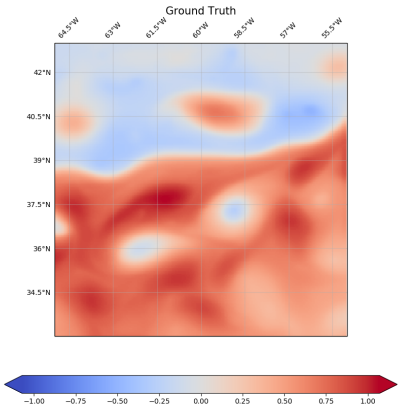

(b) Ground Truth (∇_{SSH})

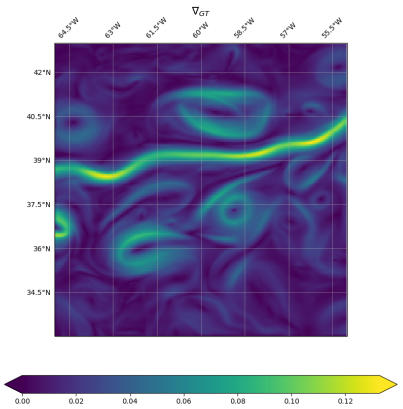

(c) Observations (nadir)

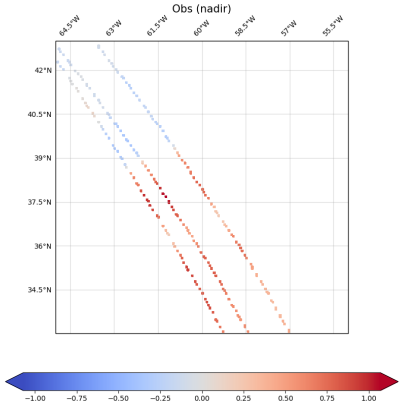

(d) Observations (nadir+swot)

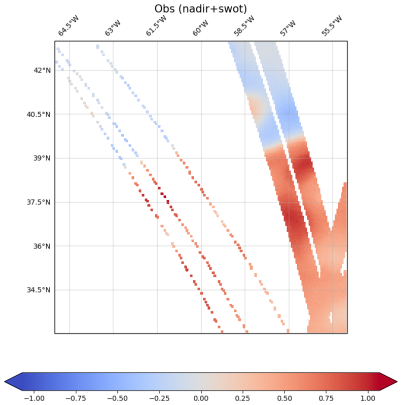

Duacs OI

DUACS OI $\overline{x}$ (Taburet et al.) as a baseline : significant smooting, solving spatial scales up to 150km :

(a) Ground Truth (∇_{SSH})

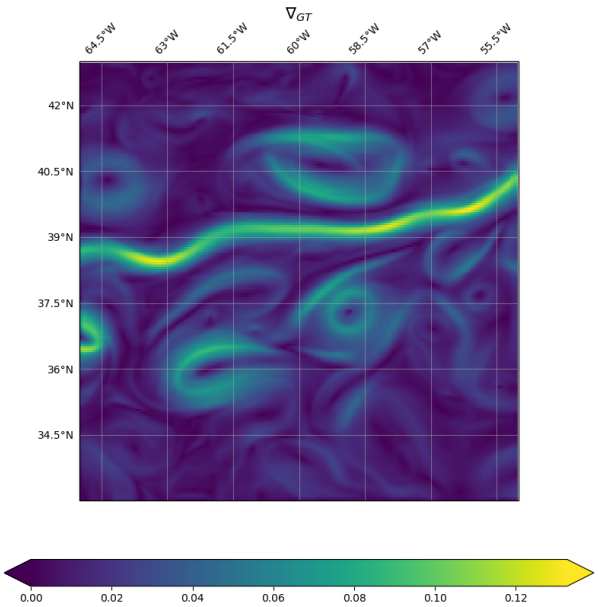

(b) OI (∇_{SSH})

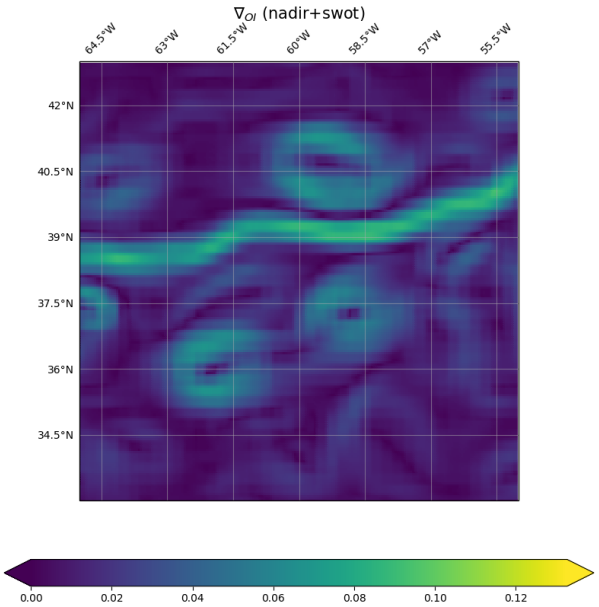

Gulfstream I

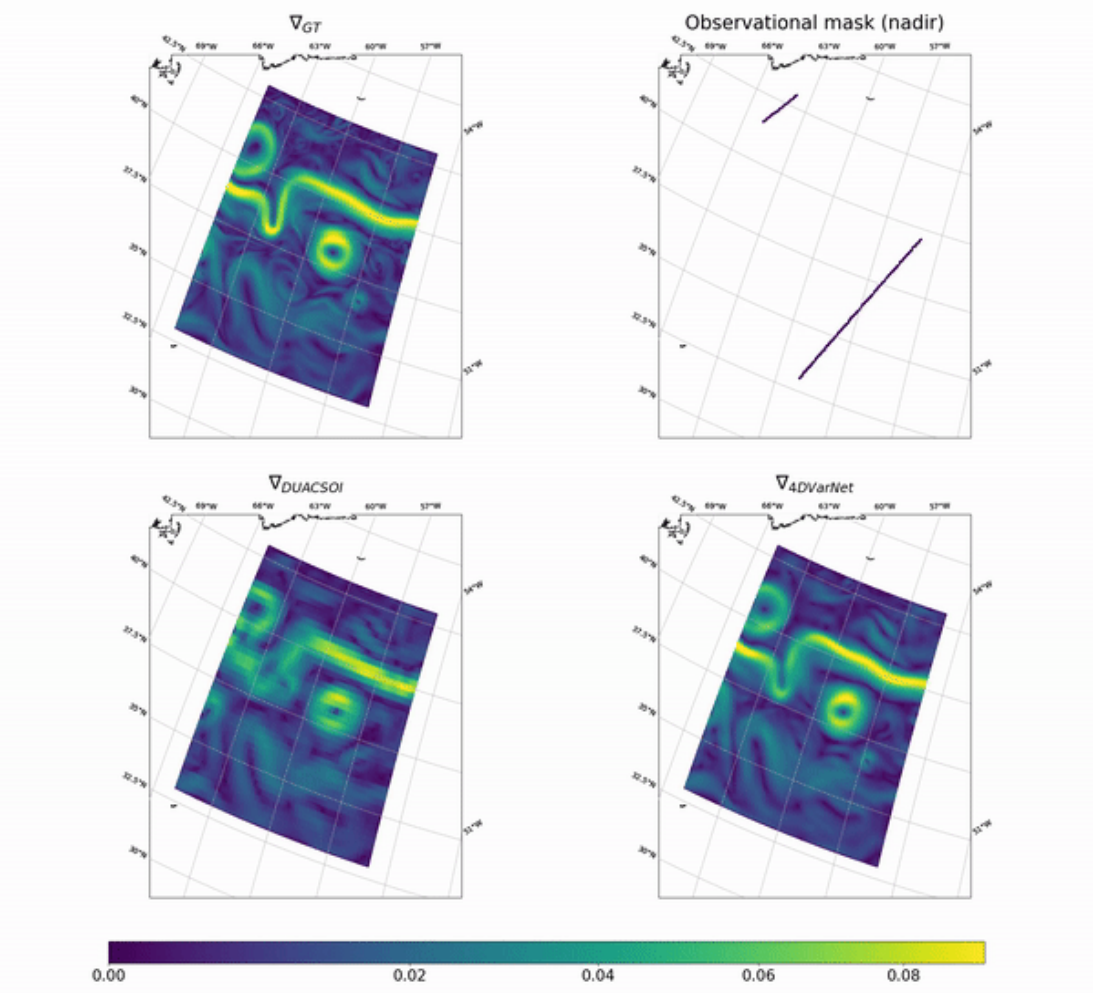

Figure: Gulfstream SSH daily interpolation

Gulfstream II

Time series

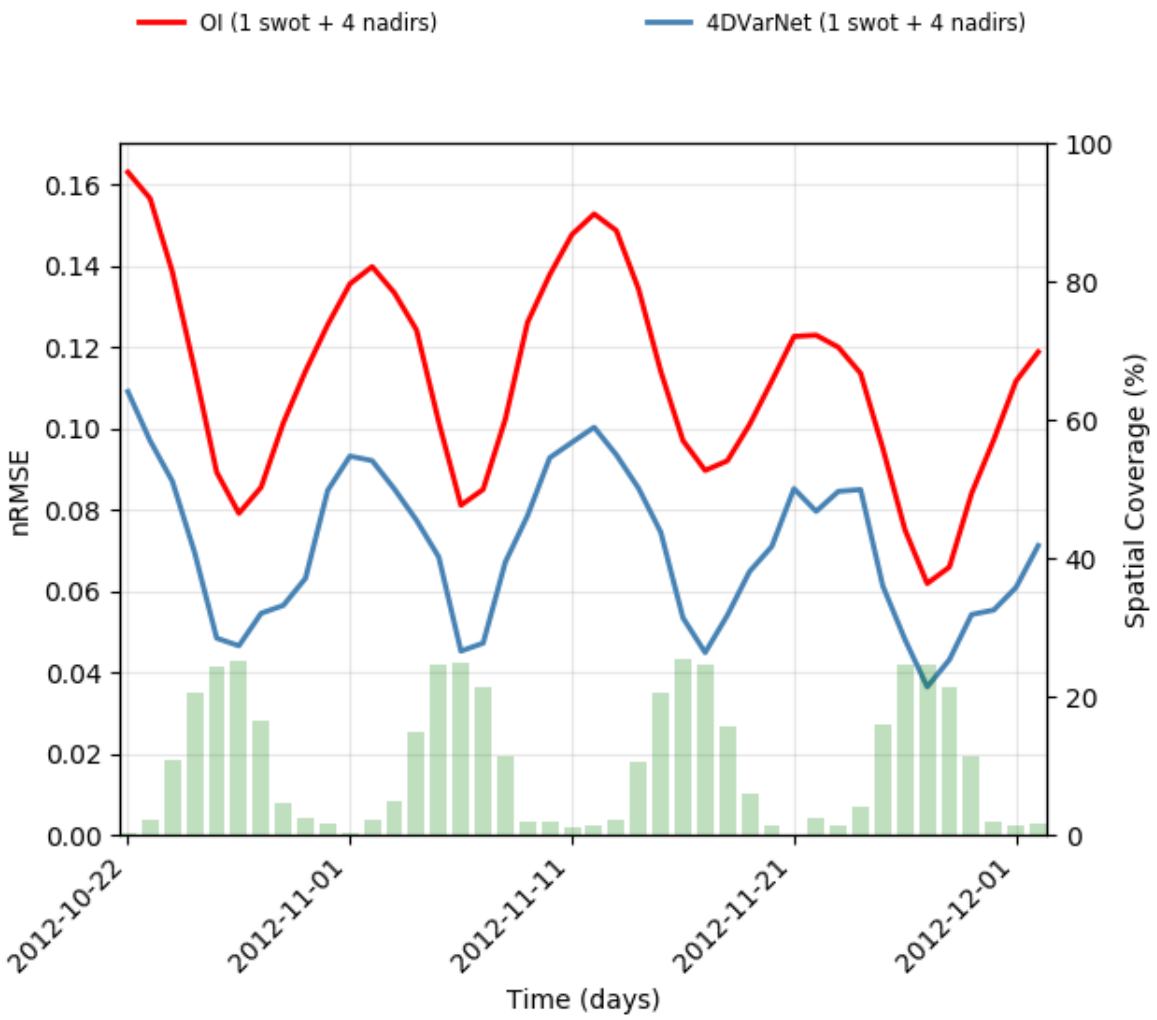

Osmosis I

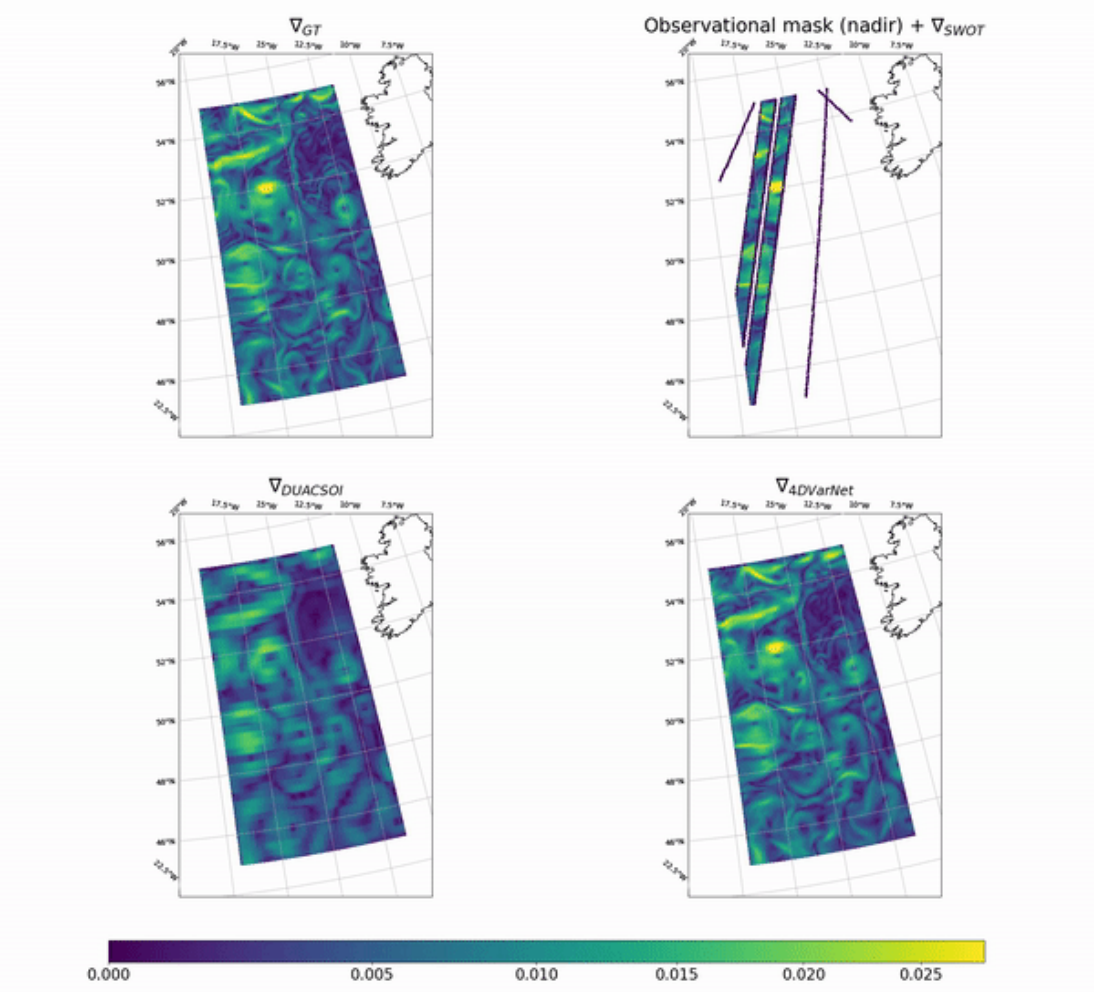

Figure: Osmosis SSH daily interpolation

Osmosis II

Time series

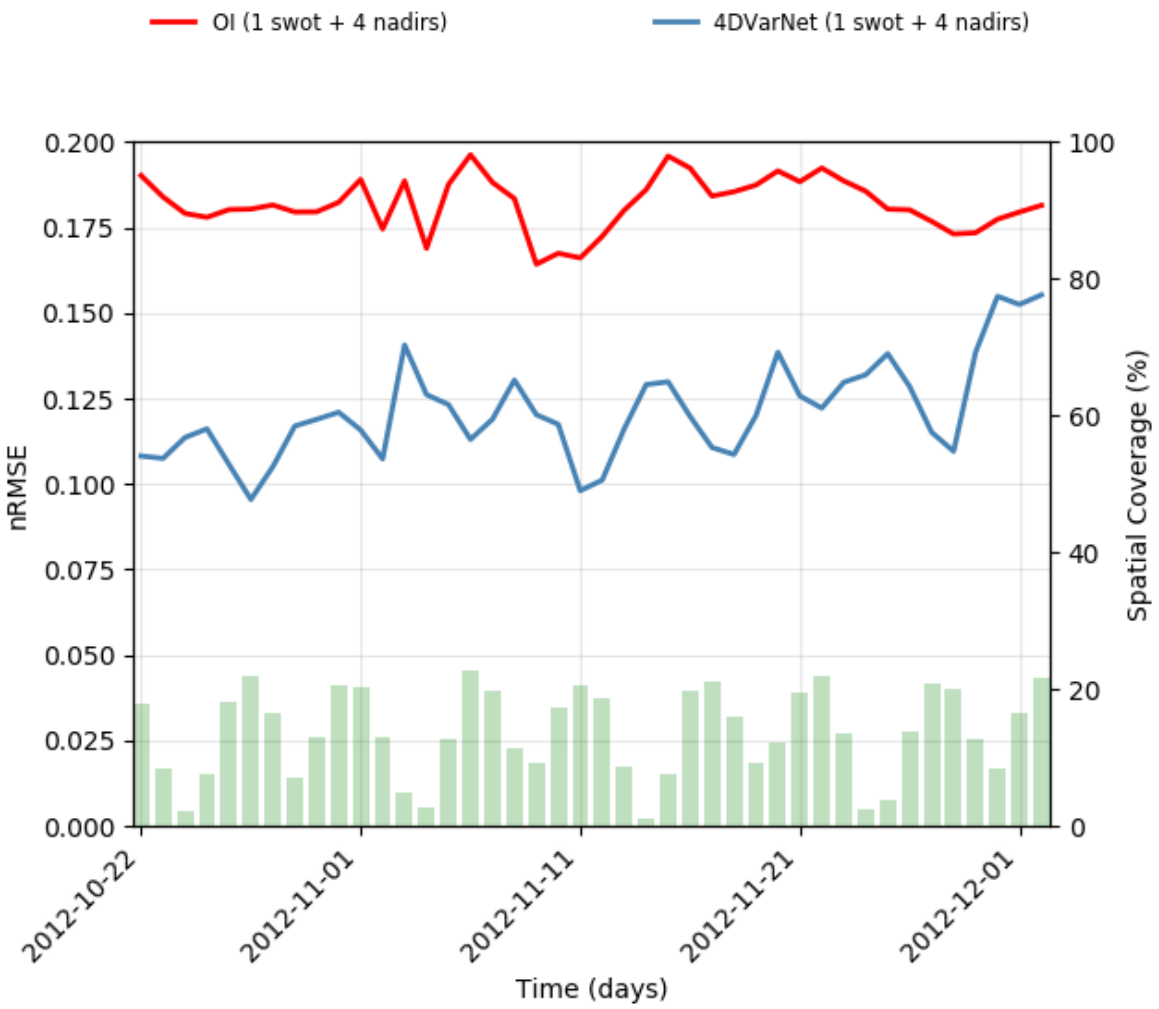

Table of contents

1 Introduction

2 Method: 4DVarNet

3 Observation System Simulation Experiment
- Experiments
- New applications

4 Observation System Experiment
- Experiments

5 Conclusion

Sparse sampling operator

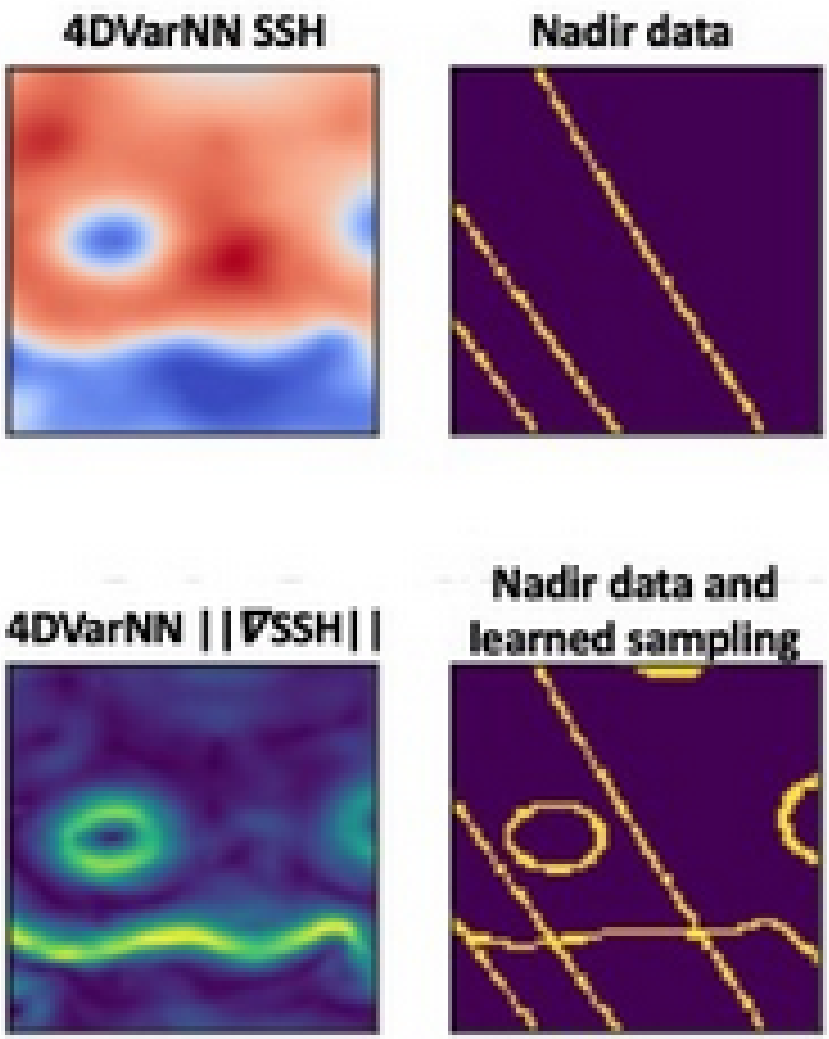

Multimodal observation

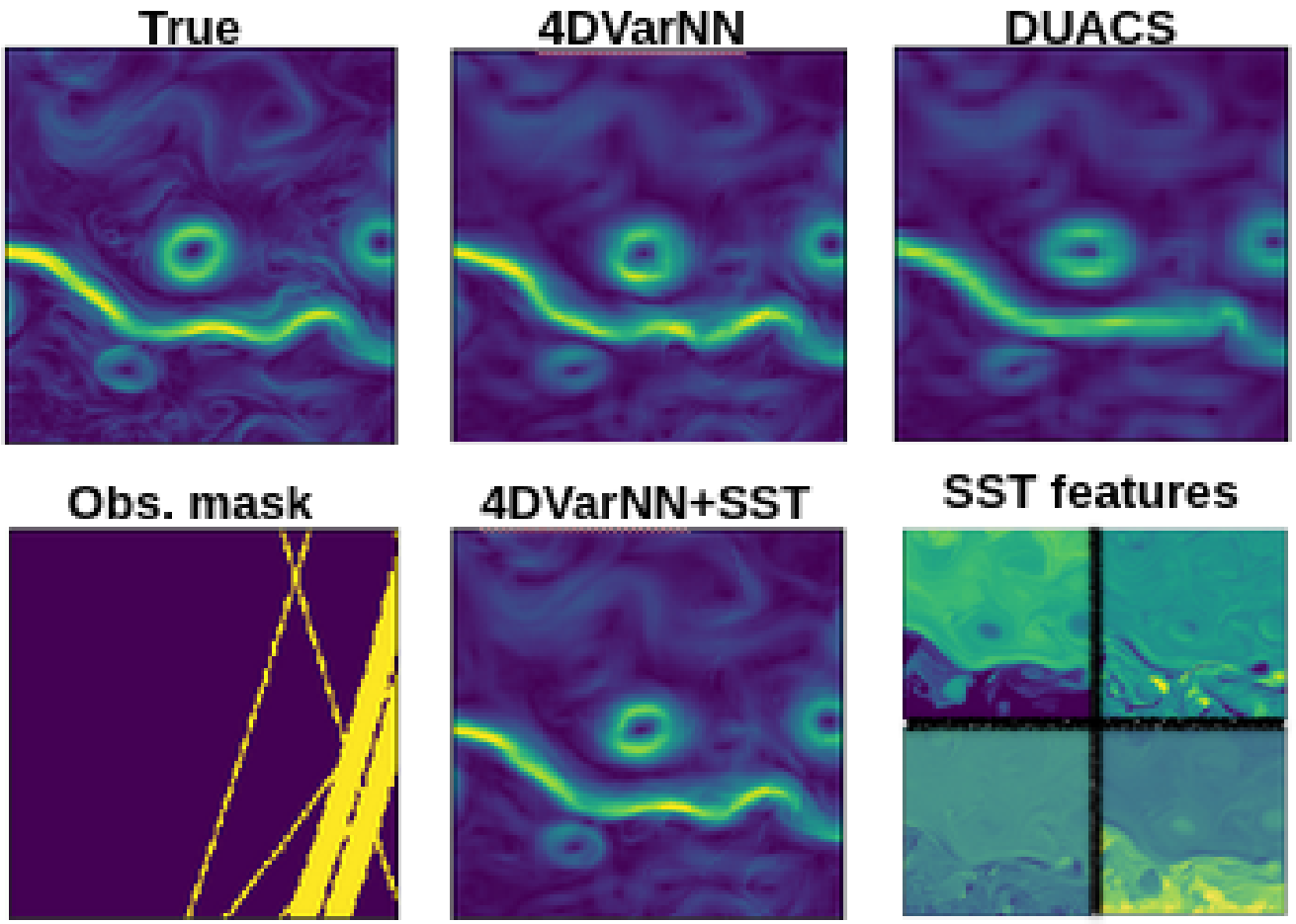

Calibration operator

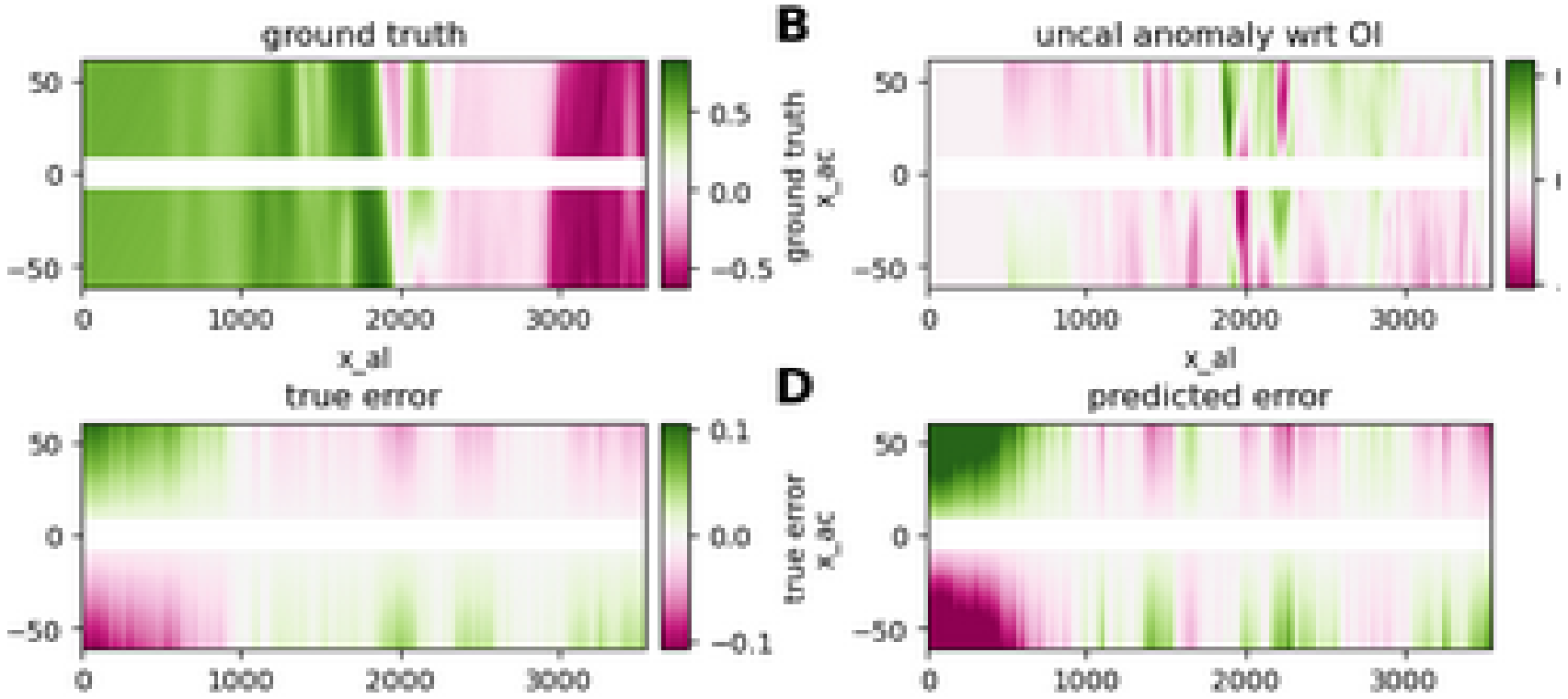

Table of contents

1 Introduction

2 Method: 4DVarNet

3 Observation System Simulation Experiment
- Experiments
- New applications

4 Observation System Experiment
- Experiments

5 Conclusion

Data

The state space formulation includes:

- a low-resolution SSH
- a high-resolution SSH anomaly

while the observation vector includes:

- OI (for the low-resolution SSH)
- the altimetric observations (Satellite observations are from real 2017 sea surface height data from altimeter)
- the SST (model-based in idealistic experiments)

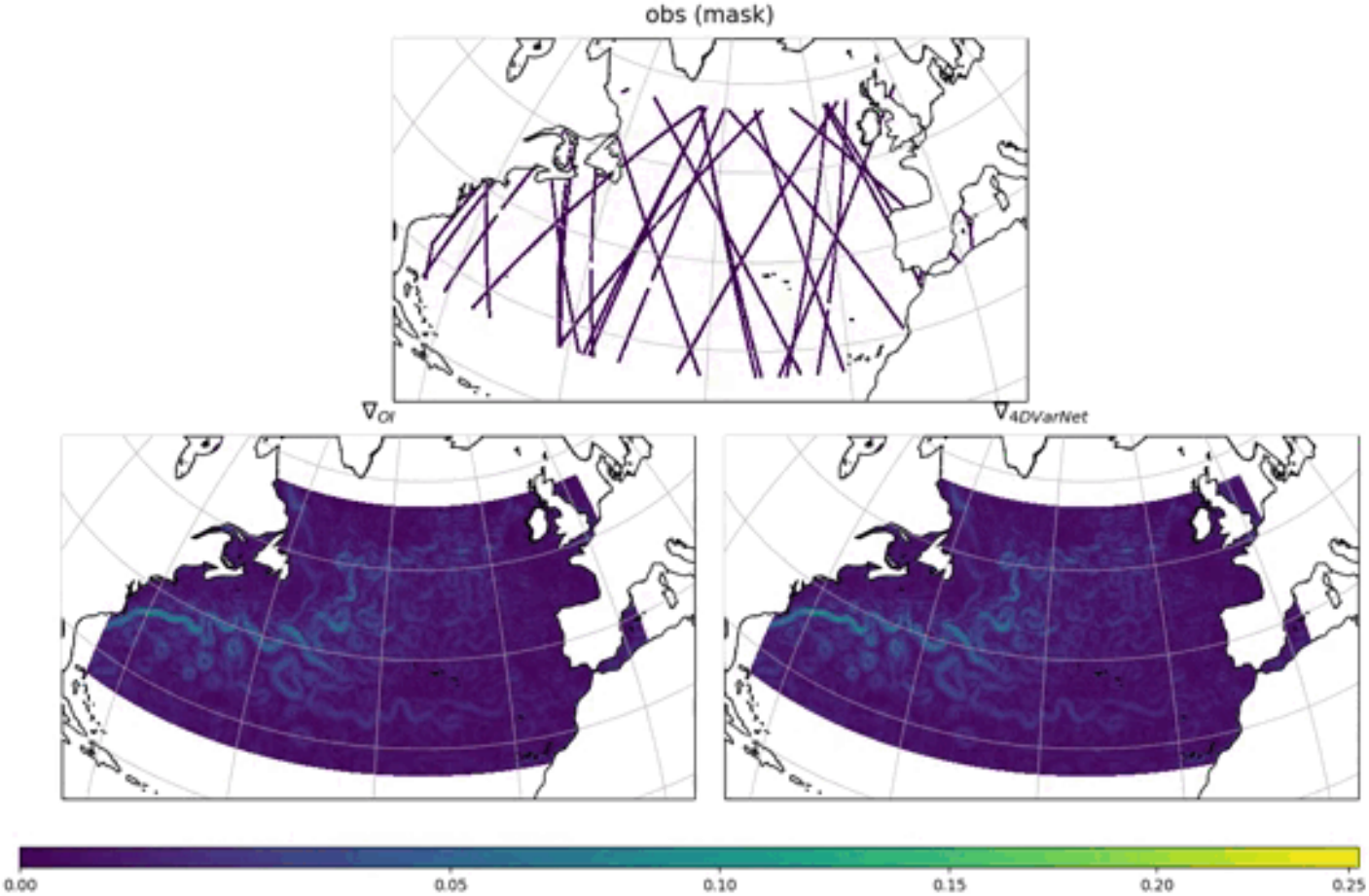

Figure: North Atlantic SSH daily interpolation (2017)

Conclusion

Done

- We can bridge DNN and variational models to solve inverse problems
- Learning jointly variational priors, observation models and solvers
- Optimal sampling as a learning issue under sparsity constraint

In progress

- **Stochastic implementation** in progress

4DVarNet code

https://github.com/CIA-Oceanix/4dvarnet-core

Annexe I: Gulfstream OSSE score

Table: 4DVarNet performance on the GULFSTREAM domain compared to DUACS OI and BFN over the period from 2012-10-22 to 2012-12-02 (42 days)

Method	μ(RMSE)	σ(RMSE)	λx (degree)	λt (days)
duacs 4 nadirs	0.92	0.01	1.42	12.0
bfn 4 nadirs	0.92	0.02	1.23	10.6
dymost 4 nadirs	0.91	0.01	1.36	11.79
miost 4 nadirs	0.93	0.01	1.35	10.19
4DVarNet 4 nadirs	**0.94**	**0.01**	**1.06**	**6.42**
duacs 1 swot + 4 nadirs	0.92	0.02	1.22	11.15
bfn 1 swot + 4 nadirs	0.93	0.02	0.8	10.09
dymost 1 swot + 4 nadirs	0.93	0.02	1.2	10.07
miost 1 swot + 4 nadirs	0.94	0.01	1.18	10.14
4DVarNet 1 swot + 4 nadirs	**0.95**	**0.01**	**0.7**	**6.34**

Annexe II: Gulfstream OSE score

Table: 4DVarNet performance on the GULFSTREAM domain compared to DUACS OI and BFN over the whole year 2017

Method	μ(RMSE)	σ(RMSE)	λx (km)
DUACS	0.88	0.07	152
MIOST	0.89	0.08	139
DYMOST	0.89	0.06	129
BFN	0.88	0.06	122
4DVarNet (SSH only)	0.88	0.08	132
4DVarNet (SSH+SST)	0.88	0.06	122

References I

M. Asch, M. Bocquet, and M. Nodet. *Data Assimilation*. Fundamentals of Algorithms. Society for Industrial and Applied Mathematics, Dec. 2016. ISBN 978-1-61197-453-9. doi: 10.1137/1.9781611974546. URL https://doi.org/10.1137/1.9781611974546.

M. Bocquet, J. Brajard, A. Carrassi, and L. Bertino. Data assimilation as a learning tool to infer ordinary differential equation representations of dynamical models. *Nonlinear Processes in Geophysics*, 26(3):143–162, 2019. doi: 10.5194/npg-26-143-2019. URL https://npg.copernicus.org/articles/26/143/2019/.

J. Brajard, A. Carrassi, M. Bocquet, and L. Bertino. Combining data assimilation and machine learning to infer unresolved scale parametrization, 2021. URL https://royalsocietypublishing.org/doi/abs/10.1098/rsta.2020.0086.

A. Carrassi, M. Bocquet, L. Bertino, and G. Evensen. Data assimilation in the geosciences: An overview of methods, issues, and perspectives. *WIREs Climate Change*, 9(5):e535, 2018. doi: https://doi.org/10.1002/wcc.535. URL https://onlinelibrary.wiley.com/doi/abs/10.1002/wcc.535.

J. Chilès and P. Delfiner. *Geostatistics : modeling spatial uncertainty*. Wiley, New-York, second edition, 2012.

G. Evensen. *Data Assimilation*. Springer Berlin Heidelberg, Berlin, Heidelberg, 2009. ISBN 9783642037108 9783642037115. URL http://link.springer.com/10.1007/978-3-642-03711-5.

F. Lindgren, H. Rue, and J. Lindström. An explicit link between gaussian fields and gaussian markov random fields: the stochastic partial differential equation approach. *Journal of the Royal Statistical Society: Series B (Statistical Methodology)*, 73(4):423–498, 2011. doi: 10.1111/j.1467-9868.2011.00777.x. URL https://rss.onlinelibrary.wiley.com/doi/abs/10.1111/j.1467-9868.2011.00777.x.

References II

P. A. O'Gorman and J. G. Dwyer. Using machine learning to parameterize moist convection: Potential for modeling of climate, climate change, and extreme events. *Journal of Advances in Modeling Earth Systems*, 10(10):2548–2563, 2018. doi: https://doi.org/10.1029/2018MS001351. URL https://agupubs.onlinelibrary.wiley.com/doi/abs/10.1029/2018MS001351.

S. Rasp, M. S. Pritchard, and P. Gentine. Deep learning to represent subgrid processes in climate models. *Proceedings of the National Academy of Sciences*, 115(39):9684–9689, 2018. ISSN 0027-8424. doi: 10.1073/pnas.1810286115. URL https://www.pnas.org/content/115/39/9684.

G. Taburet, A. Sanchez-Roman, M. Ballarotta, M.-I. Pujol, J.-F. Legeais, F. Fournier, Y. Faugere, and G. Dibarboure. DUACS DT2018: 25 years of reprocessed sea level altimetry products. 15(5):1207–1224. ISSN 1812-0784. doi: https://doi.org/10.5194/os-15-1207-2019. URL https://www.ocean-sci.net/15/1207/2019/. Publisher: Copernicus GmbH.

P. Tandeo, P. Ailliot, J. Ruiz, A. Hannart, B. Chapron, A. Cuzol, V. Monbet, R. Easton, and R. Fablet. Combining Analog Method and Ensemble Data Assimilation: Application to the Lorenz-63 Chaotic System. In V. Lakshmanan, E. Gilleland, A. McGovern, and M. Tingley, editors, *Machine Learning and Data Mining Approaches to Climate Science*, pages 3–12. Springer, 2015.

P.-Y. Traon, F. Nadal, and N. Ducet. An improved mapping method of multisatellite altimeter data. *Journal of Atmospheric and Oceanic Technology - J ATMOS OCEAN TECHNOL*, 15:522–534, 04 1998. doi: 10.1175/1520-0426(1998)015<0522:AIMMOM>2.0.CO;2.